Journal of Soils and Sediments (2026) 26:140
https://doi.org/10.1007/s11368-026-04329-2

SEDIMENTS, SEC 3 • HILLSLOPE AND RIVER BASIN SEDIMENT DYNAMICS • RESEARCH ARTICLE

Slope effects on flow resistance and soil erosion in tortuous rills

Vincenzo Palmeri[1,2] · Alessio Nicosia[1] · Costanza Di Stefano[1] · Gaetano Guida[1] · Vincenzo Pampalone[1] · Vito Ferro[1,2]

Received: 12 January 2026 / Accepted: 20 March 2026

Abstract

Purpose Even though rill erosion is strongly influenced by flow hydraulics, slope, and channel tortuosity, the influence of path tortuosity on rill flow resistance and soil erosion has been investigated little. In this study, experiments on tortuous rills were performed on a plot with a mean slope s_p of 15% filled with clay soil to test a literature flow resistance equation previously proposed for tortuous rills and investigate if slope affects the potential link between rill tortuosity and soil loss.

Methods The four pre-shaped rills, characterized by designed tortuosity values t_0 = 1, 1.08, 1.16, and 1.3, were subjected to a constant inflow discharge (0.3 L s^{-1}), and the hydraulic variables were measured using the dye-tracing technique and 3D digital terrain models obtained by terrestrial surveys performed before and after the runs. Soil erosion volumes were quantified through DEMs (Digital Elevation Model) of difference. This analysis was also carried out for the experimental runs of a previous investigation with the same experimental setup and s_p = 11%.

Results The results confirmed that the literature flow resistance equation can be satisfactorily applied to estimate flow resistance in tortuous rills, and that tortuosity effects can be effectively captured by the a coefficient of the power velocity distribution regardless of the plot mean slope. The obtained results also revealed that lower slope (11%) unexpectedly produced higher flow velocities (except for the maximum tortuosity level) and soil losses, which can be mostly explained by the differences in channel bed roughness generated during the shaping phase.

Conclusion Overall, this study highlights that slope influences rill hydraulics and erosion for tortuous rills. These insights advance the understanding of rill dynamics and support the refinement of predictive models for soil conservation.

Keywords Rill erosion · Soil loss · Flow resistance · Tortuosity · Rill morphology

1 Introduction

Globally, soil erosion is a serious issue due to its on-site and off-site effects, such as losses in soil fertility and agricultural productivity, river and reservoir over-sedimentation, and degradation of water quality (Borrelli et al. 2017; Carollo et al. 2023a; Di Stefano et al. 2023). In terms of soil loss, the rill component frequently predominates over the interrill (Bruno et al. 2008; Liu et al. 2011; Di Stefano et al. 2013, 2022a). Therefore, studies on rill erosion are fundamental for the development and assessment of predictive models aimed at evaluating the need for soil management strategies and thus suggesting effective soil conservation measures. Rills are small eroded channels, which rapidly change their own morphology and strictly depend on the interplay between flow and soil surface microtopography (Foster et al. 1984; Di Stefano et al. 2022b). For bare hillslopes, rills naturally tend to develop linearly along the maximum slope direction, but for hillslopes with sparse and unevenly arranged vegetation (i.e., shrubs), the soil supporting vegetated patches is often elevated compared to the surrounding area, and runoff is forced to flow between patches (Nouwakpo et al. 2016). In this case, the rill path deviates from the straight one and

Responsible editor: Rebecca Bartley

✉ Alessio Nicosia
alessio.nicosia@unipa.it

[1] Department of Agricultural, Food and Forest Sciences, University of Palermo, Viale Delle Scienze, Building 4, 90128 Palermo, Italy

[2] National Biodiversity Future Center, NBFC, 90133 Palermo, Italy

Published online: 09 April 2026

is characterized by a certain degree of tortuosity. The tortuosity of a rill is a quantitative indicator of its morphology and represents the deviation of the thalweg from a straight channel alignment (Strohmeier et al. 2014).

The knowledge of flow hydraulic variables, such as mean flow velocity V (Govers 1992; Di Stefano et al. 2021; Nicosia et al. 2021) and hydraulic radius R, and a model that uses them to simulate sediment detachment and transport are necessary to modeling rill erosion (Gilley et al. 1990; Govers et al. 2007). Several soil erosion models regarding channelized flow use uniform flow equations, such as Darcy–Weisbach, Manning, or Chezy's (Gilley et al. 1990), originally designed for rivers (Govers et al. 2007). These flow resistance equations apply to turbulent and uniform open-channel flow (Chow 1959), from which rill flows can differ because of the geometrical scale, soil erosion, sediment transport (Nearing et al. 1997), and, in the abovementioned cases, path tortuosity. At the state of the art, even if several studies (e.g., Khatua et al. 2011; Moharana et al. 2013) have been conducted to investigate how the path shape influences flow resistance for meandering channels, this effect has been scarcely studied for rills. To the best of our knowledge, only two studies (Strohmeier et al. 2014; Carollo et al. 2023b) regarding the relationship between rill tortuosity and flow resistance are available in the literature.

Strohmeier et al. (2014) performed steady-state experiments in a sloping (slope s = 10%) flume on rills incised in loam soil (19% clay, 49% silt, and 32% sand) and studied the influence of rill tortuosity on rill flow resistance, which was expressed by the Manning–Strickler coefficient. In particular, the tortuosity parameter was calculated using top-view images of the flume by two-dimensional tracking of the mass center of a dye tracer in the flow, neglecting vertical channel bed irregularities. They performed experimental measurements using two discharge values (0.145 and 0.170 L s^{-1}) for both Free Developed Rills (FDR, unconstrained rill erosion on a plane soil bed) and Straight Constrained Rills (SCR, concentrated flow erosion in a prepared straight initial rill). For the FDR experiments, the rill flow path tortuosity varied from 1.051 to 1.109, while, for the SCR experiments, it was always close to 1.000 (1.000–1.017). According to their findings, Strohmeier et al. (2014) stated that a regression model of rill tortuosity and roughness can be used to assess local friction loss of a non-uniform rill flow, thus reducing the uncertainty of the Manning–Strickler roughness coefficient.

Carollo et al. (2023b) performed a plot investigation on four rills incised in two sloping plots filled with clay (62% clay, 26.4% silt, and 11.6% sand) and clay-loam (32.7% clay, 30.9% silt, and 36.4% sand) soil and having a plot mean slope, s_p, of 11 and 18%, respectively. The first aim of their study was to establish optimal accuracy in measuring the rill thalweg to determine the actual tortuosity parameter t. Their results showed that, among the different tested cross-section spacing values, d = 0.075 m was the optimal one to determine rill tortuosity. In the place of the designed tortuosity values, t_0, of 1 (straight rill), 1.08, 1.16, and 1.30, they determined actual t values of 1.04, 1.07, 1.17, and 1.31 for the clay soil and 1.04, 1.10, 1.18, and 1.29 for the clay-loam one. The second aim of the study by Carollo et al. (2023b) was to determine the relationship between flow resistance and tortuosity and assess the reliability of a theoretical flow resistance law for tortuous rills, having more complex flows in comparison with those of straight channels, as they are characterized by velocity components in all three directions. In detail, the following theoretical law to calculate the Darcy-Weisbach friction factor f for rill flows, derived by the integration of a power velocity distribution (Carollo et al. 2021; Di Stefano et al. 2022b), was tested:

$$f = 8\left[\frac{2^{1-\delta}\Gamma Re^{\delta}}{(\delta+1)(\delta+2)}\right]^{-2/(1+\delta)} \tag{1}$$

in which δ = 1.5/ln Re (Castaing et al. 1990; Barenblatt 1991), $Re = \frac{Vh}{\nu}$ is the Reynolds number, where h is the water depth and ν is the water kinematic viscosity, and Γ is the velocity profile parameter. As reported by Di Stefano et al. (2022b), the measured Γ value, Γ_v, can be expressed as follows:

$$\Gamma_v = \frac{V}{u_*\left(\frac{u_*\alpha h}{\nu}\right)^{\delta}} \tag{2}$$

where $u^*=(gRs)^{0.5}$ is the shear velocity, g is the gravitational acceleration, R is the hydraulic radius, s is the slope steepness, and α is a function of δ (Ferro 2017; Nicosia et al. 2022a). Instead, the Γ_v parameter can be estimated by the following power equation (Di Stefano et al. 2022b):

$$\Gamma_v = \frac{aF^b}{s^c} \tag{3}$$

in which $F = \frac{V}{\sqrt{gh}}$ is the Froude number, and a, b, and c are coefficients to be determined by the available measurements.

The findings by Carollo et al. (2023b) highlighted, for both the investigated soils, a non-monotonic relationship between t and the Darcy-Weisbach friction factor f, but with differences in the magnitude of the friction factor between

the two cases. Specifically, the f values of the clay loam soil were higher than those related to the clay soil, and this result was mainly attributed to different slope ranges rather than soil effect. The obtained non-monotonic trend was explained as the result of the interplay among three flow resistance components due to bed roughness, sediment transport, and localized energy losses due to curves. Finally, they positively tested the applicability of Eqs. (1) and (3) for tortuous rills and found that the predicted friction factor was dependent on t. In detail, as the soil effect on the friction factor was considered negligible, the available measurements for the two soils were used together to calibrate Eq. (3), obtaining $b=1.070$, $c=0.466$, and a varying with t in the range 0.50-0.53.

Also, the effects of rill path tortuosity on soil erosion have been little investigated. Shen et al. (2015) presented the concept of rill tortuosity complexity, calculated as the ratio between the total length of a rill and its bifurcations to its vertical (i.e., accounting for the vertical direction along the hillslope) effective length. In particular, they studied the influence of simulated rainfall intensity on rill network development. Their results showed that rill tortuosity complexity depends on rainfall intensity, while it has only a weak relationship with soil loss. Shen et al. (2019), studying the effects of simulated rainfalls on rill development and characteristics for loessial soil, found that the increase of rill tortuosity complexity promoted erosion due to sidewall collapse and determined higher rill width-depth ratios. Finally, He et al. (2023), who performed rainfall simulation experiments on a sloping flume, found that soil erosion amount does not depend on rill tortuosity complexity.

Therefore, the analysis of the few available literature studies highlighted the necessity to further investigate how rill path tortuosity affects flow resistance and soil erosion. Moreover, to the best of our knowledge, the slope effects on flow resistance and soil erosion for tortuous rills have not been studied.

In this study, plot experiments on tortuous rills were conducted using the same clay soil of the study by Carollo et al. (2023b) and a plot mean slope of 15%. The experimental flow resistance measurements of this study were used with the main aim of testing the flow resistance equation proposed by Carollo et al. (2023b). Instead, the soil loss measurements, obtained by the 3D models generated after the terrestrial survey of the plots for the experimental runs of this study and those of Carollo et al. (2023b), were used to investigate if slope affects the potential link between rill tortuosity and soil loss. Finally, the possible interaction between erosion processes and flow resistance was explored.

2 Materials and methods

The experimental runs were performed on a plot (width 2 m and length 7 m) (Fig. 1a) placed at the Department of Agriculture, Food, and Forest Sciences of the University of Palermo. This plot was filled with the same clay soil (clay = 62.0%, silt = 26.4%, sand = 11.6%) used by Carollo et al. (2023b) reaching a mean slope $s_p=15\%$. Four rills were manually incised to obtain tortuous paths characterized by designed tortuosity values, t_0, of 1 (straight rill), 1.08, 1.16, and 1.30 (Fig. 1). According to the concept of rill tortuosity

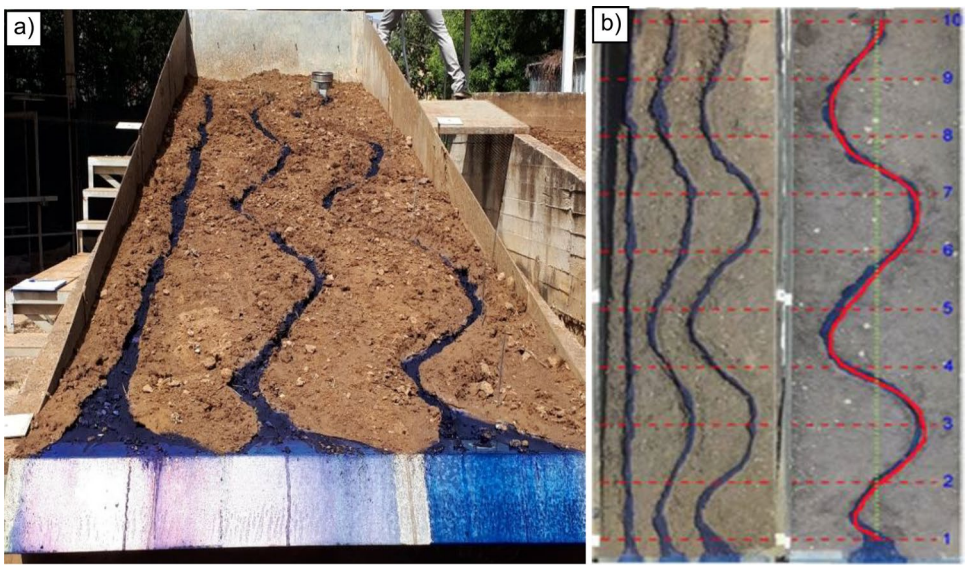

Fig. 1 View of the plot with rill channels marked by the Methylene blue solution (**a**) and plan view of four rills with different tortuosity and the ten transects (**b**). In the right part of the figure, the red line indicates the actual rill length while the green line indicates the straight length measured between its bounding sections. Rill tortuosity t is the ratio between these two lengths

given by Strohmeier et al. (2014) and Carollo et al. (2023b), also in this study, t is defined as the ratio between the actual thalweg length and the minimum (straight) length, measured between its bounding sections. The four rills were divided into nine longitudinal segments bounded by 10 transects perpendicular to the maximum plot slope and placed at a given distance (0.624 m) (Fig. 1b). The rill portion between a given transect-thalweg intersection and the rill end defined a rill reach. Consequently, each rill has nine reaches.

The manually incised rills were pre-shaped by a low clear flow discharge Q of 0.1 L s^{-1}, while for the experimental runs, a constant inflow discharge Q of 0.3 L s^{-1} was applied. The adopted experimental procedure (i.e., a pre-shaping phase with Q=0.1 L s^{-1} and the subsequent experimental run with Q=0.3 L s^{-1}) does not allow performing comparable replicate runs. This limitation arises because the rill channel that develops during the pre-shaping phase results from the dynamic interaction between the flow and the manually incised initial rill. Consequently, it is not possible to obtain identical rill channels once the pre-shaping phase is completed. In other words, runs with replicated rills having a fixed rill tortuosity were not performed, as the mobile-bed channel obtained by a manually incised rill and subsequent pre-shaping phase cannot be recreated with the same initial geometry. Therefore, the effects due to the natural variability related to the channel modeling by flow cannot be considered, since a perfect replicate of a tortuous channel, obtained by manual incision and pre-shaping phase, cannot be obtained.

The dye-tracing technique (Govers 1992; Abrahams et al. 1996; Di Stefano et al. 2021) was used to measure the mean rill flow velocity V. A small volume of Methylene blue solution was injected in the transect-thalweg intersection to measure, by a chronometer, the travel time of the leading edge of the dye cloud over the reach length. The ratio between the reach length and the travel time to cover this length gave the surface velocity V_s of the leading edge. The reach length was accurately measured along the thalweg extracted from the final 3D model, as reported below. The V_s value was corrected by a factor of 0.8 (Zhang et al. 2010; Carollo et al. 2021) to obtain the corresponding mean flow velocity V.

Before (after the shaping phase) and after the experimental runs, the plot was surveyed (approximately 70 photographs) by a digital camera to create the three-dimensional Digital Terrain Models (3D-DTM). These pictures were taken guaranteeing that all parts of the surveyed plot area were represented in at least three photographs, as the 3D algorithm is projected for working with convergent images. These photos were processed by Agisoft Photoscan Professional with an automatic process that combines the Structure from Motion (SfM) and MultiView-Stereo techniques (Di Stefano et al. 2022b).

Firstly, the 3D-DTM after the experimental runs (Q=0.3 L s^{-1}) was used to establish the rill channel geometry and determine the actual tortuosity t. From the final 3D-DTM, an approximate rill thalweg was tracked by photointerpretation. Then, applying a specific calculation routine, the cross-sections perpendicular to this rill thalweg and spaced 0.075 m apart were tracked, and the lowest point of each cross-section was identified. The actual rill thalweg was the line joining these points (Fig. 1b). This interdistance value (0.075 m) was used according to the findings by Carollo et al. (2023b), who demonstrated that it was the most physically sound. In this study, the actual t values of the examined rills were equal to 1.02 (straight rill), 1.08, 1.16, and 1.28. The slope steepness s of a given reach was obtained as the mean of the values measured in the rill reach thalweg extracted by 3D-DTM.

The raster obtained as the difference between the 3D-DTM before and after the experimental runs (DEM of difference, DoD) was used for calculating the scour depth and the consequent eroded soil volume Y (m^3) for each rill. The eroded soil volumes were also calculated for the experimental runs presented in the paper by Carollo et al. (2023b) for which the 3D-DTM before and after the experimental runs were available. For both the survey performed in this study and that by Carollo et al. (2023b), the longitudinal profiles of the rill thalweg were determined by using the Digital Elevation Models (DEMs) after the rill shaping phase and after the conclusion of the experimental runs. Both the longitudinal profiles before and after the runs were used to determine the roughness depth values RD (i.e., the differences in height between the longitudinal profile before or after the experiments and the corresponding reference straight line joining the upstream and the downstream cross-sections of the rills) (Fig. 2).

The hydraulic radius R and water depth h values of each rill reach were determined by the technique proposed by Di Stefano et al. (2019), which combines the ground survey of the rill from the SfM technique and the survey of the water tracks inside the channel marked by a dye solution. In particular, a Methylene blue solution was injected into the flow to mark the rill tracks (Fig. 1a) and allow the survey of the wetted lateral surface SL_{rr} by applying the GIS functions "real surface" (SAGA 7.0.0) and "zonal statistics" (ArcGIS 10.5). Starting from the vector polygon corresponding to the rill tracks, the water surface was created by the ArcGIStool

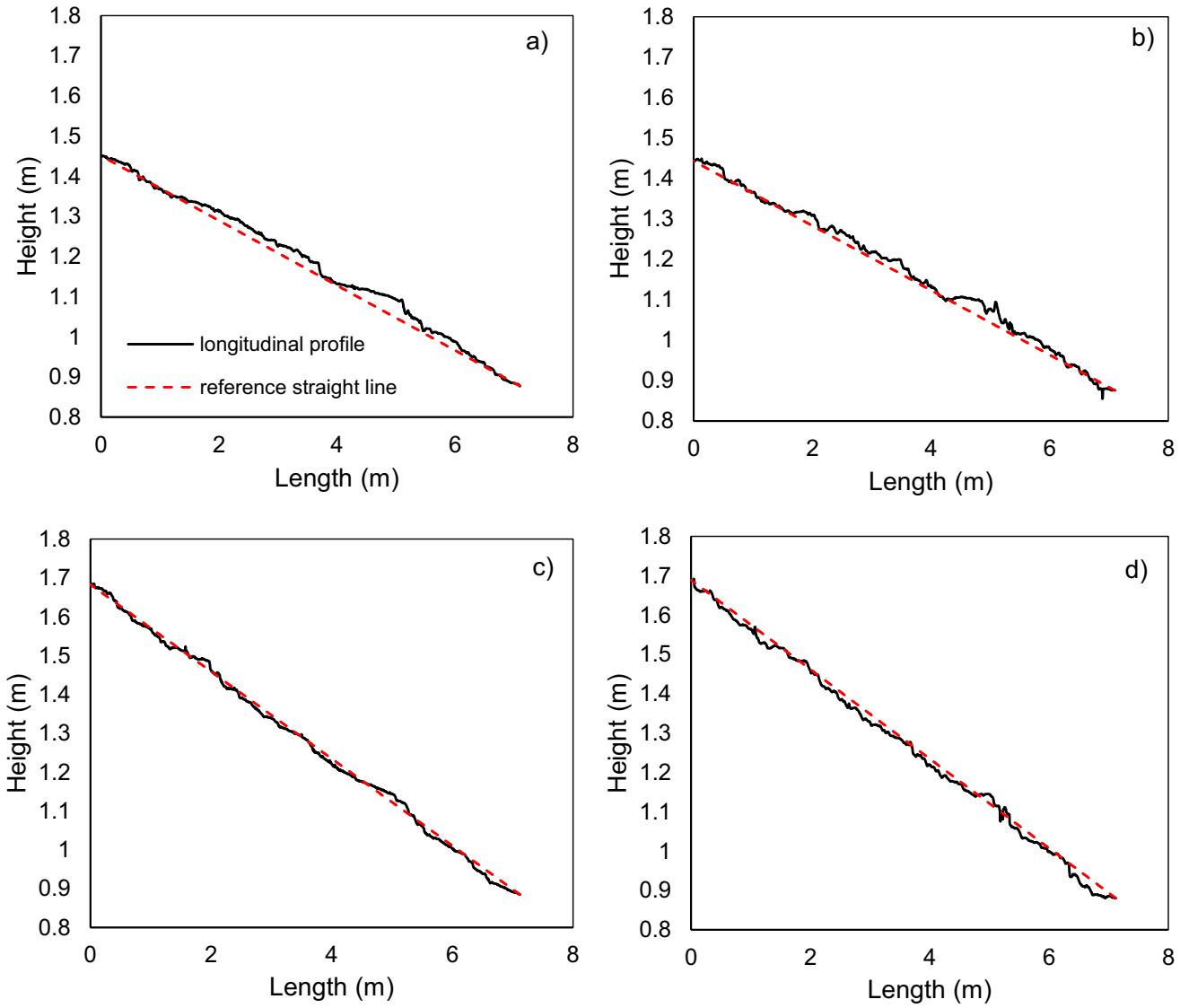

Fig. 2 Examples, for $t_0 = 1.3$, for $s_p = 11\%$ (**a** and **b**) and 15% (**c** and **d**), of the rill thalweg longitudinal profile before (**a** and **c**) and after (**b** and **d**) the experimental runs. The dotted line represents the corresponding reference straight line joining the upstream and the downstream cross-sections of the rills used to determine the roughness depth *RD*

implemented by Báčová et al. (2019), and the corresponding area W_{rr} was measured. The difference between the DTM of the reconstructed water surface and that of the eroded channel was used to obtain the channel volume V_{rr}. Therefore, the mean hydraulic radius R and water depth h were obtained by applying the following equations (Carollo et al. 2023b):

$$R = \frac{V_{rr}}{SL_{rr}} \tag{4}$$

$$h = \frac{V_{rr}}{W_{rr}} \tag{5}$$

The final 3D-DTMs were also used to obtain the rill plan area A (m^2). All the hydraulic and geometric measurements of each rill reach were used to calculate the Darcy-Weisbach friction factor $f = \frac{8gRs}{V^2}$, the Froude number F, and the Reynolds number Re. A total of 36 measurements were collected, resulting from four rills with nine reaches. The Reynolds number varied from 3689 to 5877; therefore, the rill flow was always fully turbulent. The Froude number varied from 0.95 to 1.76, and the flow was supercritical for 32 out of 36 cases.

The experimental runs of this study ($s_p = 15\%$) will be compared with the analogues results obtained by Carollo et al. (2023b) using the same clay soil and a plot mean

slope of 11%. The obtained results and the meaning of this comparison are obviously affected by the investigated s_p range.

3 Results

3.1 Analysis of the flow characteristics

Figure 3 shows the relationships between the main geometric and hydraulic variables (s, R, V, and f) and the rill tortuosity t for the whole rill channels (i.e., from the inlet to the outlet section) for the experimental runs of this study (s_p = 15%). For allowing the comparison, this figure also plots the data (s_p = 11%) already published in the paper by Carollo et al. (2023b). For both cases, it is worth noting that the lengthening of the thalweg for a given difference in elevation due to an increased path tortuosity determined the expected slope reduction (Fig. 3a). In particular, for s_p = 15%, the mean rill slope decreased from 14.8% for the straight rill channel (t = 1.02) to 11.1% for t = 1.28, whereas, for s_p = 11%, the mean rill slope decreased from 10.7% for the straight rill channel (t = 1.04) to 8.3% for t = 1.31. The hydraulic radius (Fig. 3b) is practically constant (0.01 m) for both cases, while both the flow velocity (Fig. 3c) and the friction factor (Fig. 3d) fluctuate across different tortuosity values. In particular, for this study (s_p = 15%), f reaches the maximum for the straight rill and the minimum for the highest level of tortuosity, while, in Carollo et al. (2023b) (s_p = 11%), f reached the maximum for the highest level of tortuosity and the minimum for t = 1.17.

The differences in terms of flow velocity and Darcy-Weisbach friction factor can be further investigated by a direct comparison of all the measurements (reach scale) obtained for the two s_p values. For the main hydraulic variables (V, h, F, and f), Fig. 4 shows the comparison between the values obtained for s_p = 15% and s_p = 11%. It is worth noting that the series with t_0 = 1, 1.08, and 1.16 have the same pattern, while that with t_0 = 1.3 behaves differently. In particular, mean flow velocity (Fig. 4a), water depth (Fig. 4b), and Froude number (Fig. 4c) values of s_p = 11% tend to be higher than those obtained for s_p = 15%, except for t_0 = 1.3. On the contrary, for t_0 = 1.3, the Darcy-Weisbach friction factor values (Fig. 4d) for

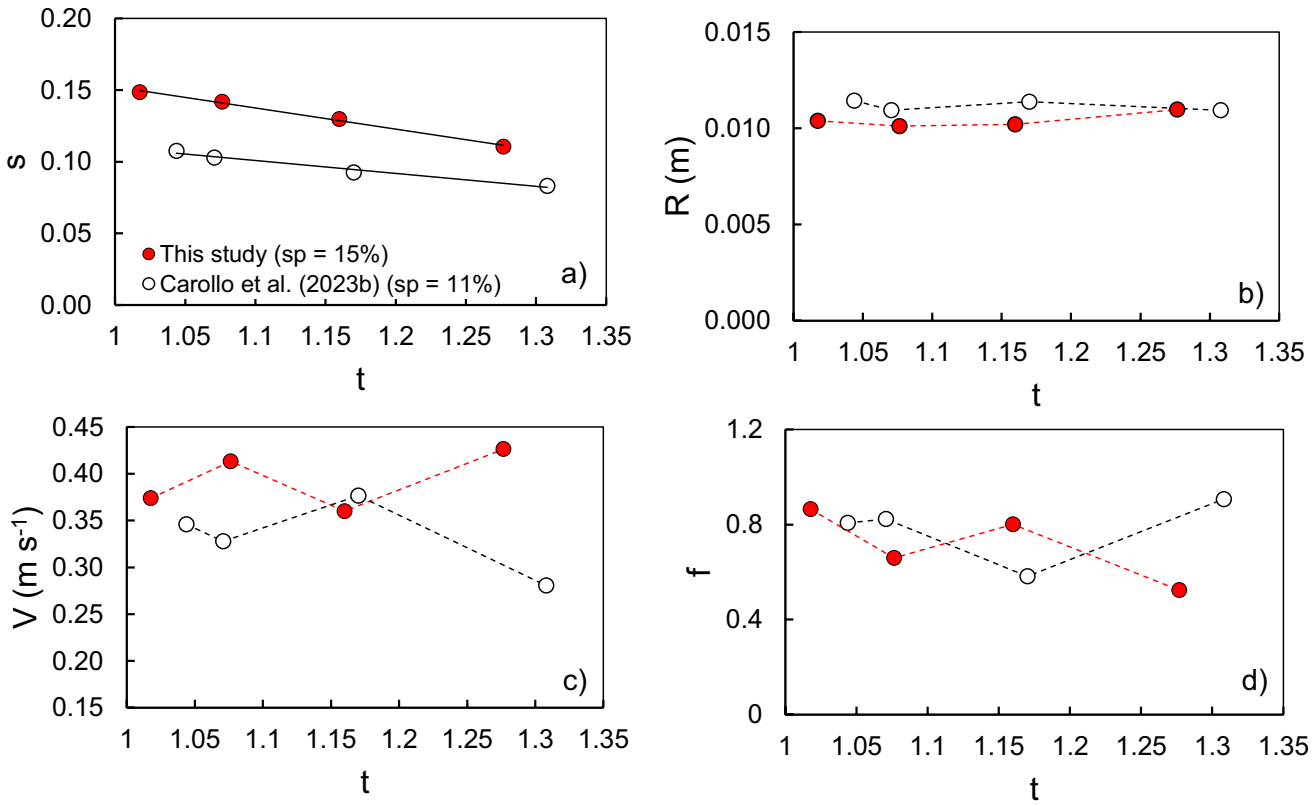

Fig. 3 Experimental values of rill thalweg slope s (**a**), hydraulic radius R (**b**), mean flow velocity V (**c**), and Darcy-Weisbach friction factor f (**d**) with tortuosity t for the four entire rill channels of this study

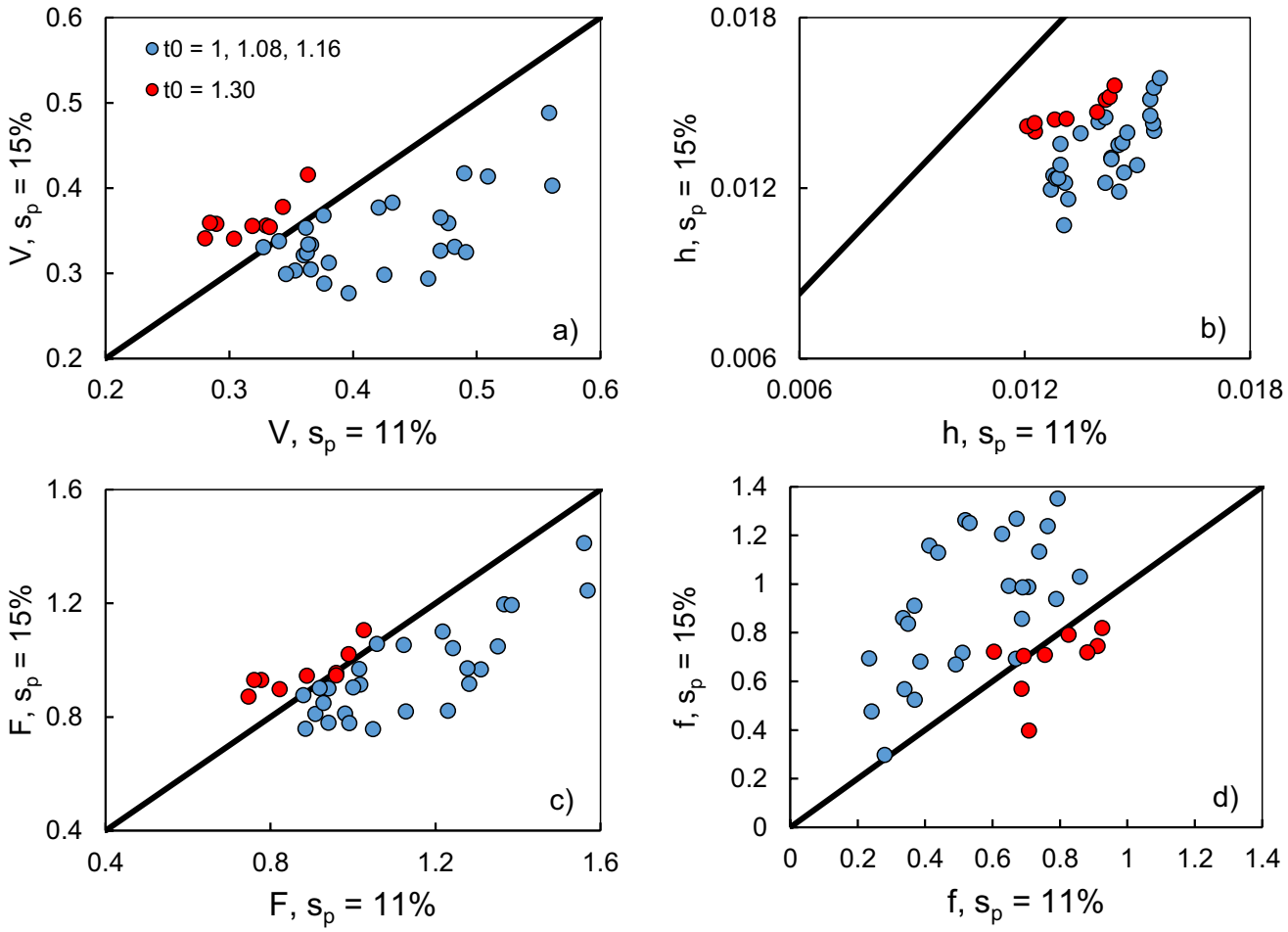

Fig. 4 Comparison between the values of V (**a**), h (**b**), F (**c**), and f (**d**) obtained for $s_p = 15\%$ and $s_p = 11\%$

$s_p = 15\%$ tend to be lower than those for $s_p = 11\%$, while the other levels of tortuosity are characterized by higher flow resistance for $s_p = 15\%$.

3.2 Testing the flow resistance law developed for tortuous rills

The measurements at the reach scale of flow velocity V, hydraulic radius R, slope s, and water depth h were used to assess the flow resistance law (Eqs. 1 and 3) calibrated by Carollo et al. (2023b). In detail, the coefficients b and c of Eq. (3) were set to 1.070 and 0.466, respectively, while the tortuosity effect was exclusively attributed to the a coefficient. For each t value, a was determined as the slope coefficient of the best-fit straight line to the ($F^{1.070}/s^{0.466}$, Γ_v) pairs (where the experimental Γ_v are obtained by Eq. 2) passing through the origin of the axes (Fig. 5a). For the four increasing t values, a was equal to 0.519, 0.509, 0.505, and 0.522, respectively. It is worth noting that these values fall within the range (0.50–0.53) previously obtained by Carollo et al. (2023b) for both the investigated soils. Thus, Eqs. (1) and (3), with $b = 1.070$, $c = 0.466$, and the abovementioned a values, were tested. Figure 5b shows the comparison between the measured f values and those calculated by the relationship proposed by Carollo et al. (2023b) (Eqs. (1) and (3), with $b = 1.070$, $c = 0.466$) introducing the a value obtained for each tortuosity level. The proposed approach gives excellent friction factor estimations, as the mean absolute error is equal to 1.4%, and 35 out of 36 estimate errors are lower than ± 5% (Fig. 5b).

The a values obtained in this study (0.505–0.522, with a mean value of 0.514) are very similar to those (0.504–0.512, with a mean value of 0.509) reported by Carollo et al. (2023b) for the same clay soil and $s_p = 11\%$. This result implies that this coefficient could be considered independent of the plot mean slope. For this reason, the abovementioned analysis was repeated by joining the experimental runs performed in this study and those by Carollo et al.

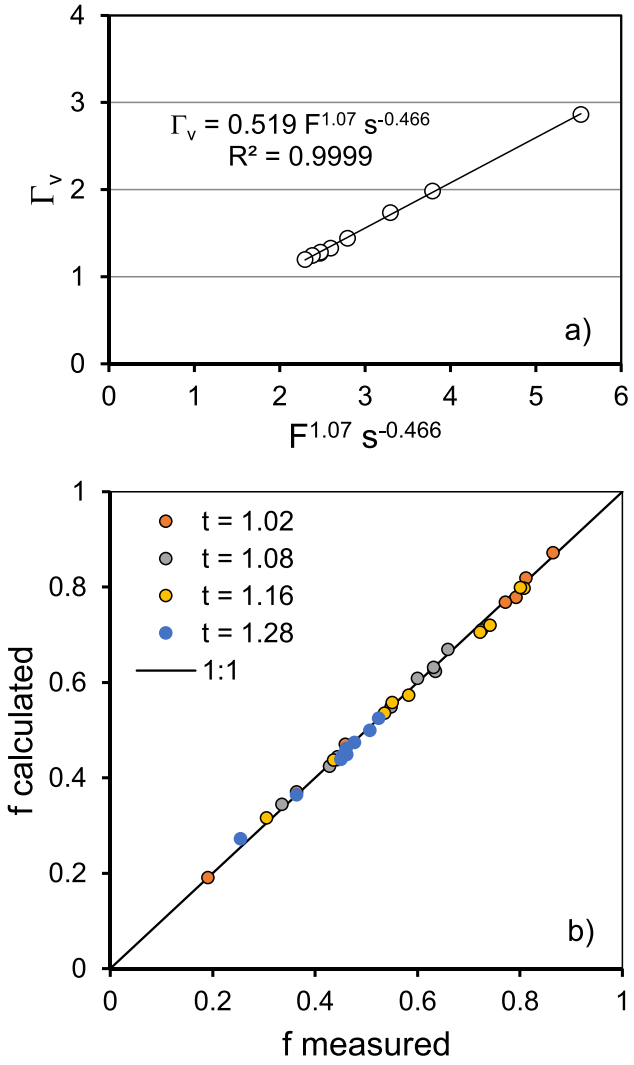

Fig. 5 Pairs ($F^{1.070}/s^{0.466}$, Γ_v) for the straight rill (**a**) and comparison between the measured values of the Darcy Weisbach friction factor and the predicted ones by Eq. (1) and Eq. (3) with $b=1.070$, $c=0.466$, and a values depending on t obtained only for the runs of this study (**b**)

(2023b) regardless of the plot mean slope. Also in this case, for each t_0 value, a was determined as the slope coefficient of the best-fit straight line to the ($F^{1.070}/s^{0.466}$, Γ_v) pairs (where the experimental Γ_v are obtained by Eq. 2) passing through the origin of the axes, obtaining $a=0.514$, 0.506, 0.509, and 0.519 for the four increasing t_0 values. Figure 6 shows the comparison between the measured f values and those calculated by the relationship proposed by Carollo et al. (2023b) (Eqs. (1) and (3), with $b=1.070$, $c=0.466$) introducing the new a coefficients ($a=0.514$, 0.506, 0.509, and 0.519) obtained for each t_0 value. Also in this case, the friction factor estimates obtained by the proposed approach are excellent, with a mean absolute error equal to 1.94%, and 65 out of 66 estimate errors are lower than ± 5%.

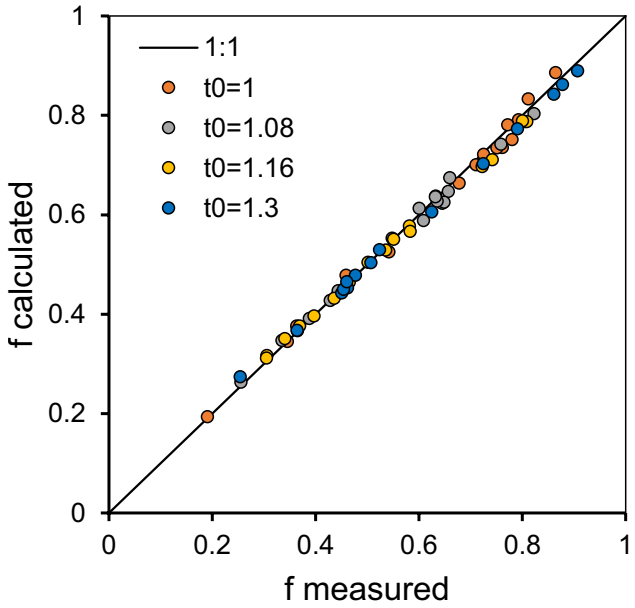

Fig. 6 Comparison between the measured values of the Darcy Weisbach friction factor and the predicted ones by Eq. (1) and Eq. (3) with $b=1.070$, $c=0.466$, and a values depending on t_0 obtained by joining the runs of this study and those by Carollo et al. (2023b)

3.3 Soil erosion in tortuous rills with different slopes

For $s_p=15\%$, Fig. 7a shows that, for increasing values of the tortuosity, the eroded volume first decreases, then increases, and finally decreases again. This pattern is the same as that which was detected for the friction factor (Fig. 3d). Instead, for $s_p=11\%$, Fig. 7a shows that Y decreases with increasing tortuosity level. In this case, the pattern does not follow that detected for the friction factor (Fig. 3d), since, for the maximum tortuosity ($t=1.31$), the highest Darcy-Weisbach friction factor value is obtained.

Figure 7a also demonstrates that $s_p=11\%$ is characterized by higher values of eroded volume than $s_p=15\%$ for all the tortuosity values. This result can also be visualized by observing the DoDs obtained for the two plot mean slope values (Fig. 8). However, Fig. 7b reveals that these differences tend to flatten, especially for $t_0=1$ and 1.16, when considering the soil eroded volume per unit of rill volume (Y/Ah) values. Figure 8, which also shows the spatial distribution of the scour depth along the rill channel, points out that, for $s_p=15\%$, the increased eroded volume in the passage from $t=1.08$ to 1.16 is mainly due to the different erosion processes that occurred in the mid-downstream part of the rills, and that for $t=1.28$ the erosion process was of little significance throughout the rill channel. Instead, for $s_p=11\%$, no significant differences of the scour depth spatial distribution among the four rills can be observed, except for

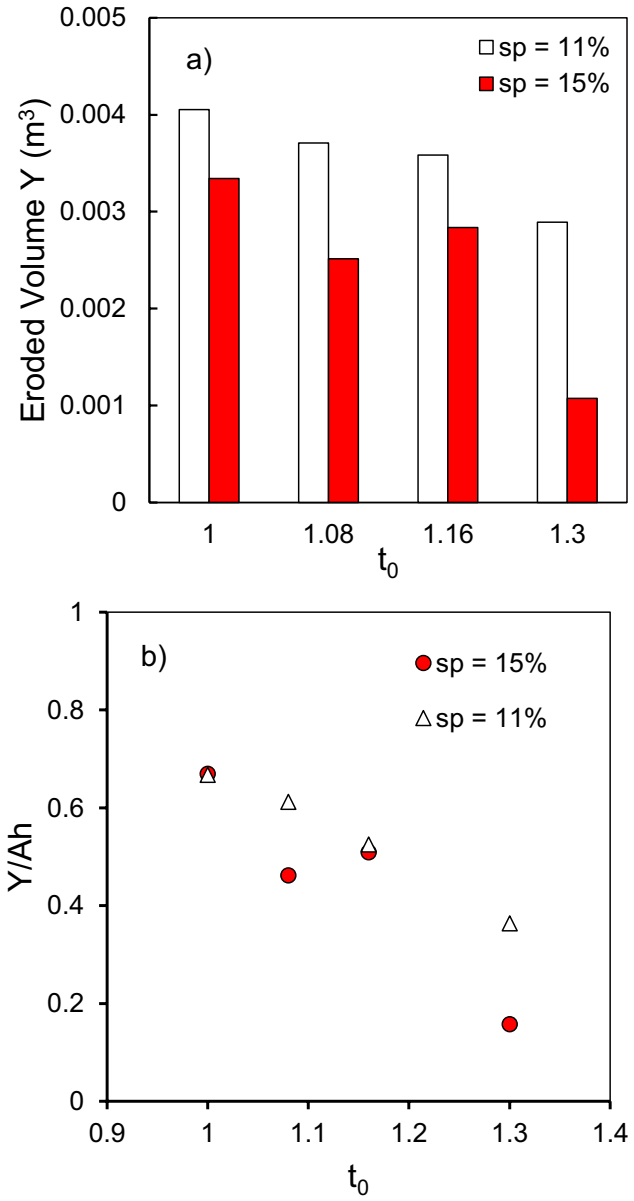

Fig. 7 Values of the eroded volume Y (**a**) and eroded volume per unit of rill volume Y/Ah (**b**) along the entire rill across different tortuosity values for the experimental runs of this study (s_p=15%) and by Carollo et al. (2023b) (s_p=11%)

t=1.31 for which the highest scour depths are not localized in the mid-downstream part of the rill.

4 Discussion

4.1 Testing the flow resistance law developed for tortuous rills

The results shown in Fig. 5b confirmed that the relationship proposed by Carollo et al. (2023b) (Eqs. (1) and (3), with b=1.070, c=0.466), introducing the a value obtained for each tortuosity level, leads to an accurate estimate of the Darcy-Weisbach friction factor (errors less than or equal to ± 5% for 97.2% of the examined cases) also for the experimental runs of this study.

Moreover, the comparison between the a values obtained in this study and those obtained by Carollo et al. (2023b) for the same clay soil highlighted that this coefficient can be considered independent of the investigated plot mean slope and strictly depends on the rill tortuosity. Indeed, the Darcy-Weisbach friction factor estimates obtained by using the a value obtained for each t_0 value joining the runs of this study and those by Carollo et al. (2023b) (Fig. 6) remain excellent, with errors less than or equal to ± 5% for 98.5% of the examined cases. These findings mean that the flow resistance law can be satisfactorily applied to estimate flow resistance in tortuous rills with different slopes, attributing the variability due to different tortuosity levels exclusively to the a coefficient.

However, this result could be affected by the circumstance that the two investigated plot mean slopes are close. For this reason, these findings should be further tested for other experimental runs performed in tortuous rills developed in the same soil with a different plot mean slope.

4.2 Flow characteristics and soil erosion in tortuous rills with different slopes

The analysis of the main hydraulic variables (Fig. 4) pointed out that the mean flow velocity values for s_p=11% are always higher than those for s_p=15%, with the only exception of t_0=1.3 (Fig. 4a). Moreover, flow resistance (Fig. 4d) for s_p=15% is higher than s_p=11% for t_0 from 1 to 1.16, while the opposite pattern is detected for t_0=1.3. For fixed conditions (rill shaping procedure, soil, applied flow discharge, and tortuosity levels), it is expected that a higher plot mean slope value determines higher flow velocities and, consequently, higher eroded volumes. However, the findings of this study contradict this hypothesis, showing higher values of both mean flow velocities (except for t_0=1.3) (Fig. 4a) and eroded volumes (Figs. 7a and 8) for the lowest plot mean slope.

According to the additive flow resistance model, the total friction factor is given by the sum of the three components due to bed grain roughness, sediment transport, and localized energy losses due to curves. The first two components should increase depending on the magnitude of the erosion process (Govers 1992; Giménez and Govers 2001), while the third is influenced by local friction effects that should increase with increasing tortuosity. Of course, total flow resistance affects flow behavior and determines differences in mean flow velocity and transport capacity, with repercussions in soil erosion.

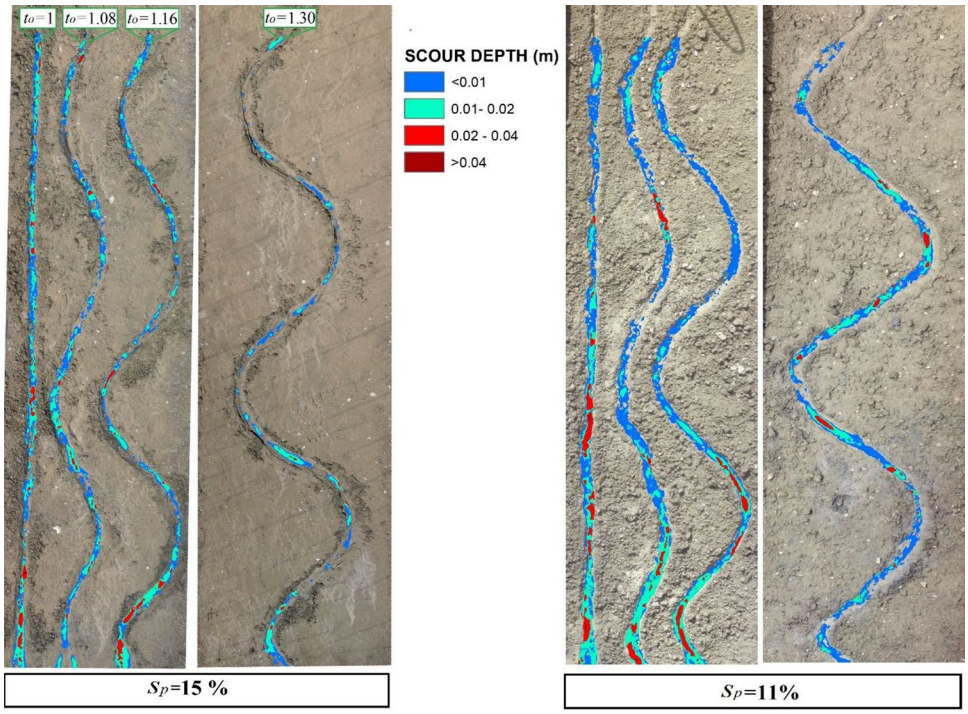

Fig. 8 Spatial distribution of the scour depth for the four rills investigated in this study (s_p=15%) and those by Carollo et al. (2023b) (s_p=11%)

For a given value of path tortuosity (i.e., a comparable f component due to curves), assuming that the component of f due to sediment transport is negligible, the differences in flow resistance can be exclusively attributed to channel shaping, which determines a roughness due to the size of the particles (bed grain roughness) and possible bedforms (e.g., step-pool). For these experimental runs (this study and Carollo et al. 2023b), the hypothesis of neglecting the flow resistance component due to sediment transport phenomena can be considered plausible, as the experimental measurements of flow velocity were carried out when the erosion processes had drastically decreased to make visible the dye cloud of Methylene blue. Moreover, no step-pool features were detected by visual inspection and analysis of the longitudinal profiles. Therefore, for the examined runs, the results are likely influenced by changes in bed grain roughness.

Figures 9, 10, 11, and 12 show the empirical frequency distribution of the roughness depth RD values for s_p=11 and 15% before (i.e., at the end of the shaping phase) (Figs. 9a, 10a, 11a, and 12a) and after the experimental runs (Figs. 9b, 10b, 11b, and 12b). These differences, studied in terms of roughness depth RD, showed that, for values of t_0 from 1 to 1.16, the flow shaping action before the experimental runs (Q=0.1 L s^{-1}) produced channel beds with comparable roughness for both plot mean slopes (Figs. 9a and 10a for t_0=1 and 1.08) or a channel bed for s_p=11% smoother than that at 15% (Fig. 11a for t_0=1.16). These patterns remain unchanged even after the experimental runs (Q=0.3 L s^{-1}) (Figs. 9b, 10b, and 11b). For fixed soil and t_0<1.3, the lower bed roughness at 11% can be explained by the feedback mechanism (Govers 1992) that occurs during the shaping phase (Di Stefano et al. 2022a). According to Giménez and Govers (2001), the independence between rill flow velocity and slope gradient in mobile bed rills can be justified by this mechanism. In fact, the expected increase of flow velocity due to an increase in slope gradient is counterbalanced by the effect of the growth of erosion rate with increasing slope. This last effect produces an increase of bed roughness, thereby slowing the flow velocity. In this study, the steeper slope (s_p=15%) initially determines higher flow velocities during the shaping phase, but this increase determines an increase in bed roughness. This difference in initial rill bed roughness (obtained after the shaping phase) determined lower velocities (Fig. 4a) and higher flow resistance (Fig. 4d) during the runs.

Instead, for t_0=1.3, the RD values determined by the shaping phase before the experimental runs (Fig. 12a) for s_p=11% was higher than that at 15%. In other words, the experimental runs performed for the maximum tortuosity value were the only ones for which the RD values were higher for the lowest slope (s_p=11%). In this case, the roughness depth takes into account the effect of both channel roughness and the longitudinal profile shape, which is slightly convex as shown in Fig. 2a and b. In other words, for t_0=1.3, for s_p=15%, the longitudinal profile can be considered uniform (Fig. 2c and d), while it becomes convex

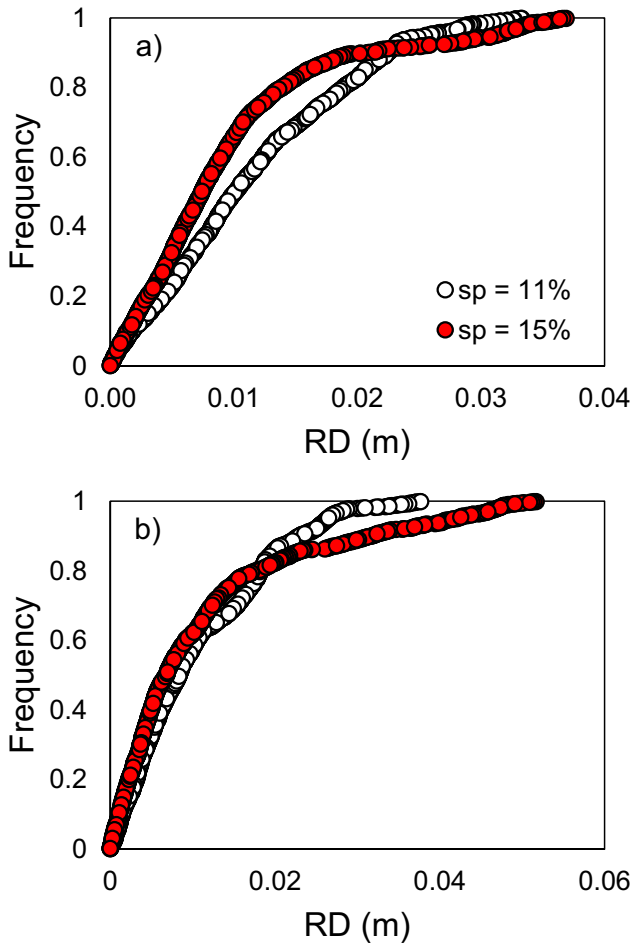

Fig. 9 Frequency distribution of roughness depth *RD* values after the shaping phase (before the experimental runs) (**a**) and after the experimental runs (**b**) for $t_0 = 1$

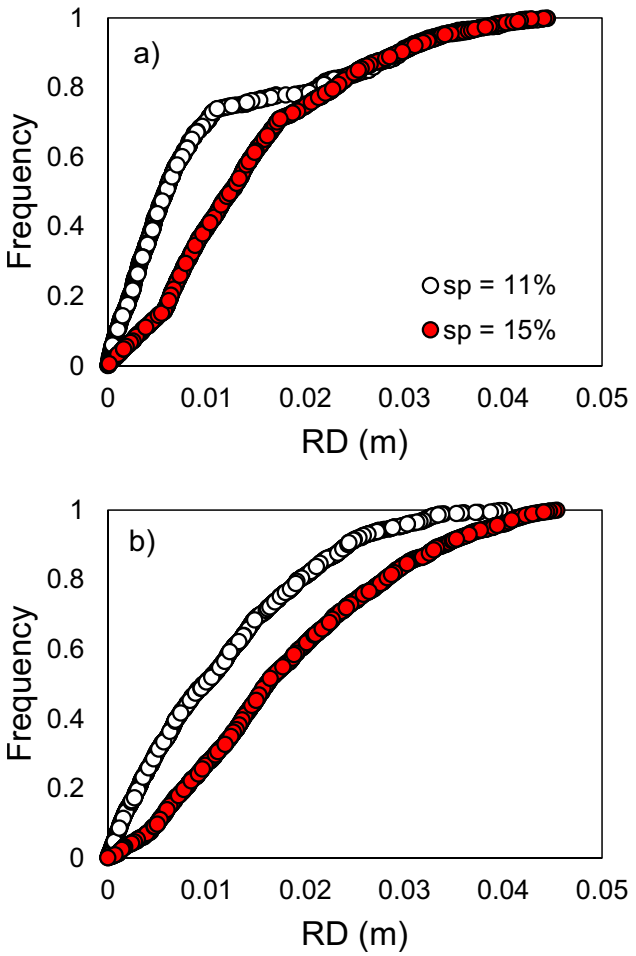

Fig. 10 Frequency distribution of roughness depth *RD* values after the shaping phase (before the experimental runs) (**a**) and after the experimental runs (**b**) for $t_0 = 1.08$

for $s_p = 11\%$. As already reported by Nicosia et al. (2022b, 2024), for fixed soil texture and slope gradient, the convex profile is characterized by higher flow resistance as compared to the uniform profile. For this reason, the Darcy-Weisbach friction factor values for $s_p = 11\%$ are higher than those for $s_p = 15\%$ (Fig. 4d).

The result that, for fixed tortuosity, the lower plot slope led to higher soil eroded volumes (Figs. 7 and 8) can be explained by the fact that, for $s_p = 11\%$, the channel beds at the beginning of the experimental run (Figs. 9a, 10a, and 11a) tends to be smoother (i.e., lower flow resistance) than those for $s_p = 15\%$, determining higher flow velocities (Fig. 4a).

It is interesting to note that, when considering eroded volume per unit of rill volume *Y*/*Ah* (Fig. 7b), the differences between the results obtained for the two investigated plot slopes flatten, especially for $t_0 = 1$ and 1.16. This result suggests that the different slope scarcely influenced the unit soil loss, while it strongly affected the magnitude of the erosion phenomena (Fig. 7a).

The main limit of this study is that the results in terms of slope effects on soil loss values for tortuous rills cannot be compared to others published in the literature, given the pioneering nature of this investigation. For this reason, further experimental runs should be carried out using other mean plot slope values in order to enlarge the investigated slope range (11–15%) and test if the observed results could likely hold under significantly lower or steeper slope conditions.

5 Conclusions

This study demonstrated that the flow resistance law proposed by Carollo et al. (2023b) can be reliably applied to tortuous rills, capturing the variability due to tortuosity by the

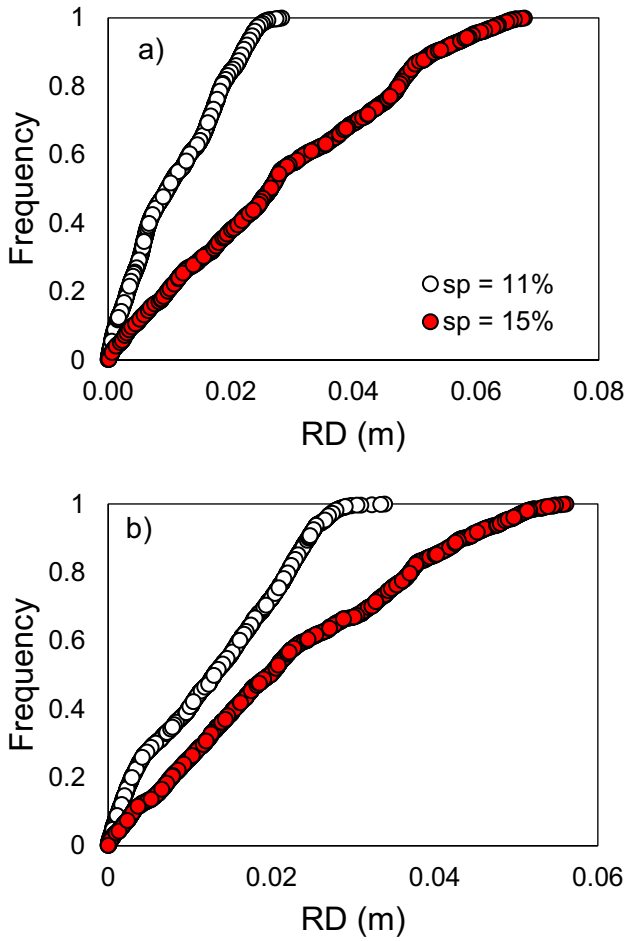

Fig. 11 Frequency distribution of roughness depth *RD* values after the shaping phase (before the experimental runs) (**a**) and after the experimental runs (**b**) for $t_0 = 1.16$

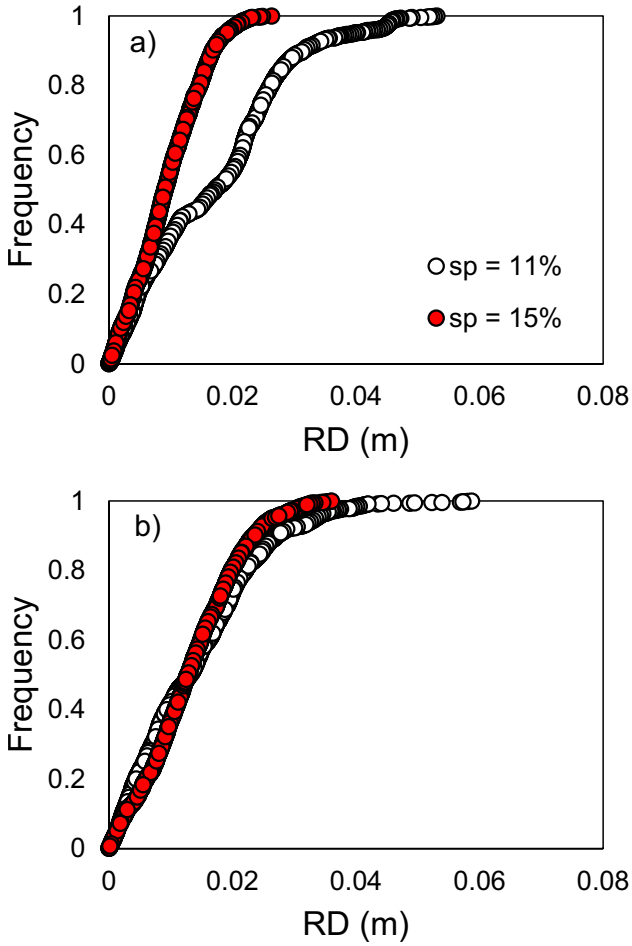

Fig. 12 Frequency distribution of roughness depth *RD* values after the shaping phase (before the experimental runs) (**a**) and after the experimental runs (**b**) for $t_0 = 1.3$

coefficient *a* regardless of the plot mean slope. The experimental results confirmed excellent agreement between measured and predicted friction factors, with errors generally below 5%.

The comparison, for fixed soil texture, between slopes of 11% and 15% revealed that lower slopes unexpectedly produced higher flow velocities and lower flow resistance, except at the highest tortuosity level. The runs for the lower slope also yielded the highest soil losses. These differences were mainly attributed to variations in channel bed roughness generated during the shaping phase (i.e., feedback mechanism), which influenced hydraulic behavior and subsequent erosion. Overall, the findings of this study highlighted that slope affects rill hydraulics and erosion for tortuous rills, strongly affecting the magnitude of erosion but only weakly influencing unit soil loss. These results emphasize the need to account for both tortuosity and slope effects when modeling rill erosion and designing soil conservation strategies. Further experiments should be performed for testing if the observed results in the investigated mean plot slope range (11%−15%) could hold under significantly lower or steeper slope conditions.

Acknowledgements All authors set up the research, analyzed and interpreted the results and contributed to write the paper. This research did not receive any specific grant from funding agencies in the public, commercial, or not- for-profit sectors.

Funding Open access funding provided by Università degli Studi di Palermo within the CRUI-CARE Agreement.

Data availability The data that support the findings of this study are available from the corresponding author upon reasonable request.

Declarations

Competing interests The authors declare that they have no known competing financial interests or personal relationships that could have appeared to influence the work reported in this paper.

References

Abrahams AD, Li G, Parsons AJ (1996) Rill hydraulics on a semiarid hillslope, southern Arizona. Earth Surf Process Landf 21:35–47. https://doi.org/10.1002/(SICI)1096-9837(199601)21:1%3c35::AID-ESP539%3e3.0.CO;2-T

Báčová M, Krása J, Devátý J, Kavka P (2019) A GIS method for volumetric assessments of erosion rills from digital surface models. Eur J Remote Sens 52(sup1):96–107. https://doi.org/10.1080/22797254.2018.1543556

Barenblatt GI (1991) On the scaling laws (incomplete self-similarity with respect to Reynolds numbers) for the developed turbulent flows in tubes. C R Acad Sci Ser II 13:307–312

Borrelli P, Robinson DA, Fleischer LR et al (2017) An assessment of the global impact of 21st century land use change on soil erosion. Nat Commun 8:1–13. https://doi.org/10.1038/s41467-017-02142-7

Bruno C, Di Stefano C, Ferro V (2008) Field investigation on rilling in the experimental Sparacia area, South Italy. Earth Surf Process Landf 33:263–279. https://doi.org/10.1002/esp.1544

Carollo FG, Di Stefano C, Nicosia A, Palmeri V, Pampalone V, Ferro V (2021) Flow resistance in mobile bed rills shaped in soils with different texture. Eur J Soil Sci 72(5):2062–2075. https://doi.org/10.1111/ejss.13093

Carollo FG, Di Stefano C, Nicosia A, Palmeri V, Pampalone V, Ferro V (2023a) A new strategy to assure compliance with soil loss tolerance at a regional scale. Catena 223:106945. https://doi.org/10.1016/j.catena.2023.106945

Carollo FG, Di Stefano C, Nicosia A, Palmeri V, Pampalone V, Ferro V (2023b) Plot investigation on rill flow resistance due to path tortuosity. Int Soil Water Conserv Res 11(4):602–609. https://doi.org/10.1016/j.iswcr.2023.02.003

Castaing B, Gagne Y, Hopfinger EJ (1990) Velocity probability density functions of high Reynolds number turbulence. Physica D 46:177–200. https://doi.org/10.1016/0167-2789(90)90035-N

Chow VT (1959) Open-channel hydraulics. McGraw-Hill Book Company, New York

Di Stefano C, Ferro V, Pampalone V, Sanzone F (2013) Field investigation of rill and ephemeral gully erosion in the Sparacia experimental area, South Italy. Catena 101:226–234. https://doi.org/10.1016/j.catena.2012.10.012

Di Stefano C, Nicosia A, Pampalone V, Palmeri V, Ferro V (2019) New technique for measuring water depth in rill channels. Catena 181:104090. https://doi.org/10.1016/j.catena.2019.104090

Di Stefano C, Nicosia A, Palmeri V, Pampalone V, Ferro V (2021) Flume experiments for assessing the dye-tracing technique in rill flows. Flow Meas Instrum 77:101870. https://doi.org/10.1016/j.flowmeasinst.2020.101870

Di Stefano C, Nicosia A, Palmeri V, Pampalone V, Ferro V (2022a) Rill flow resistance law under sediment transport. J Soils Sediments 22:334–347. https://doi.org/10.1007/s11368-021-03083-x

Di Stefano C, Nicosia A, Palmeri V, Pampalone V, Ferro V (2022b) Rill flow velocity and resistance law: a review. Earth-Sci Rev 231:104092. https://doi.org/10.1016/j.earscirev.2022.104092

Di Stefano C, Nicosia A, Pampalone V, Ferro V (2023) Soil loss tolerance in the context of the European green deal. Heliyon 9(1):e12869. https://doi.org/10.1016/j.heliyon.2023.e12869

Ferro V (2017) New flow resistance law for steep mountain streams based on velocity profile. J Irrig Drainage Eng ASCE 143(04017024):1–6. https://doi.org/10.1061/(ASCE)IR.1943-4774.0001208

Foster GR, Huggins LF, Meyer LD (1984) A laboratory study of rill hydraulics: I. velocity relationships. Trans ASAE 27:790–796. https://doi.org/10.13031/2013.32873

Gilley JE, Kottwitz ER, Simanton JR (1990) Hydraulics characteristics of rills. Trans ASAE 27:797–804. https://doi.org/10.13031/2013.31556

Giménez R, Govers G (2001) Interaction between bed roughness and flow hydraulics in eroding rills. Water Resour Res 37(3):791–799. https://doi.org/10.1029/2000WR900252

Govers G (1992) Relationship between discharge, velocity and flow area for rills eroding loose, non –layered materials. Earth Surf Process Landf 17:515–528. https://doi.org/10.1002/esp.3290170510

Govers G, Giménez R, Van Oost K (2007) Rill erosion: exploring the relationship between experiments, modeling and field observations. Earth Sci Rev 83:87–102. https://doi.org/10.1016/j.earscirev.2007.06.001

He JJ, Sun LY, Duan GY, Cai QG (2023) Slope gradient impacts on rill morphological characteristics: using indoor simulation experiment on loamy clay under certain rainfall intensity. Catena 222:106895. https://doi.org/10.1016/j.catena.2022.106895

Khatua KK, Patra KC, Nayak P (2011) Meandering effect for evaluation of roughness coefficients in open channel flow. WIT Trans Ecol Environ 146: 1743–3541. Accessed 2 Mar 2026 (WIT Press, ISSN)

Liu G, Zhang Q, Yang M (2011) Using 7Be to trace temporal variation of interrill and rill erosion on slopes. Procedia Environ Sci 11(Part C):1220–1226

Moharana S, Khatua KK, Sahu M (2013) Friction factor of a meandering open channel flow. WIT Trans Ecol Environ 172: 1743–3541. Accessed 2 Mar 2026 (WIT Press, ISSN)

Nearing MA, Norton LD, Bulgakov DA, Larionov GA, West LT, Dontsova KM (1997) Hydraulics and erosion in eroding rills. Water Resour Res 33:865–876. https://doi.org/10.1029/97WR00013

Nicosia A, Di Stefano C, Palmeri V, Pampalone V, Ferro V (2021) Roughness effect on the correction factor of surface velocity for rill flows. Hydrol Process 35:e14407. https://doi.org/10.1002/hyp.14407

Nicosia A, Palmeri V, Pampalone V, Di Stefano C, Ferro V (2022a) Slope threshold in rill flow resistance. Catena 208:105789. https://doi.org/10.1016/j.catena.2021.105789

Nicosia A, Di Stefano C, Palmeri V, Pampalone V, Ferro V (2022b) Evaluating the effects of the rill longitudinal profile on flow resistance law. Water 14(3):326. https://doi.org/10.3390/w14030326

Nicosia A, Palmeri V, Di Stefano C, Pampalone V, Guida G, Ferro V (2024) Effects of longitudinal profile shape on scour and flow resistance in rills. Eur J Soil Sci 75(4):e13561. https://doi.org/10.1111/ejss.13561

Nouwakpo SK, Williams CJ, Al-Hamdam OZ, Weltz MA, Pierson F, Nearing MA (2016) A review of concentrated flow erosion processes on rangelands: fundamental understanding and knowledge gaps. Int Soil Water Conserv Res 4:75–86. https://doi.org/10.1016/j.iswcr.2016.05.003

Shen H, Zheng F, Wen L, Lu J, Jiang Y (2015) An experimental study of rill erosion and morphology. Geomorphology 231:193–201. https://doi.org/10.1016/j.geomorph.2014.11.029

Shen H, Zheng F, Wang L, Wen L (2019) Effects of rainfall intensity and topography on rill development and rill characteristics on loessial hillslopes in China. J Mt Sci 16(10):2299–2307. https://doi.org/10.1007/s11629-019-5444-5

Strohmeier SM, Nouwakpo SK, Huang CH, Klik A (2014) Flume experimental evaluation of the effect of rill flow path tortuosity on rill roughness based on the Manning-Strickler equation. Catena 118:226–233. https://doi.org/10.1016/j.catena.2014.01.011

Zhang G, Luo R, Cao Y, Shen R, Zhang XC (2010) Correction factor to dye measured flow velocity under varying water and sediment discharges. J Hydrol 389:205–213. https://doi.org/10.1016/j.jhydrol.2010.05.050